Novel Fault Distance Estimation Method for Three-Terminal Transmission Line

Vishal Kumar Gaur, *Student member, IEEE*, Bhavesh R. Bhalja, *Senior Member, IEEE* and Mladen Kezunovic, *Life Fellow, IEEE*

***Abstract*—A new faulty section identification and fault distance estimation technique for three-terminal transmission line (TTL) is proposed in this paper. It is based on the derivation of three indices by solving non-linear equations with iterative method utilizing synchronized measurements from three ends of the line. In the absence of synchronization, an angle synchronization operator is derived for building a common reference among the three terminals. The efficacy of the technique is verified by generating several fault cases on an existing Indian 400 kV TTL using PSCAD/EMTDC software. Reported results demonstrate the capability of the presented technique for all types of fault on three-terminal transposed/untransposed as well as the non-homogeneous transmission line. It also provides accurate fault location under comprehensive variation in type of fault, line length, fault inception angle, complex fault impedance, source impedance, and current transformer (CT) saturation condition. Its accuracy remains almost constant despite errors in line parameters, as well as synchronization and noise in the measured signals. The initial guess has a minimal impact on the accuracy and convergence of the presented technique. The attained results reveal higher accuracy and better robustness of the proposed technique in comparison with those of several existing techniques.**

***Index Terms*— Three terminal transmission line, synchronized measurements, fault distance estimation, percentage error.**

I. Introduction

An accurate fault location algorithm has been a subject of great interest to achieve fast repair of transmission line and its timely restoration. Conventional fault location method, suggested for a two-terminal transmission line, cannot be directly applied on TTL due to remote infeed and involved fault path resistance [1]-[6]. In the published literature, a number of fault location methods have been proposed, which can be broadly categorized as based on (i) single-end measurement, (ii) unsynchronized/synchronized multi-end measurements. The single-end measurement-based methods utilize fundamental frequency components of voltage and/or current for fault distance estimation [7]-[9]. Though these methods are simple and economically viable, their accuracy might be affected by current infeed and fault and system parameters. Conversely, methods based on unsynchronized multi-end measurements make use of post fault voltage and current phasors to locate transmission line faults [10], [11]. Though the said methods provide better accuracy compared to methods based on single end measurement, inaccurate result during symmetrical faults is the major factor that restricts their feasibility.

Developments in the field of Phasor Measurement Units (PMUs) have introduced numerous fault location methods based on synchronized multi-end measurements. These techniques can be classified based on the traveling wave, wavelet transform, S-transform, electromechanical wave oscillation, and symmetrical components. The time of first traveling wave received at the relaying point has been utilized for fault distance estimation by the traveling wave-based schemes [12-17]. Regardless of their higher accuracy, they would not be able to detect the fault that occurs near zero inception point on account of insignificant magnitude of transient components. Besides, they require a high sampling rate to capture signal transients. Wavelet and S-transform can be effectively used for estimation of fault location on a two and/or TTL by analyzing low as well as high-frequency components generated at the time of a fault [18]-[22]. Fault detection and localization schemes for TTL based on the calculation of indices are presented in [23]-[25]. However, these algorithms may fail to locate the fault near or exactly at the junction of three line-sections. Besides, their accuracy might be affected due to a change in the equivalent source impedance.

Synchrophasor based backup distance protection schemes for estimation of fault distance on a TTL are proposed in [26]. The technique may produce significant errors for far-end low resistance fault due to consideration of an imaginary part of the line impedance. Later on, a fault location method based on the arrival time of electromechanical-wave oscillation is proposed in [27]. Although this method depends on sparse PMU measurements that do not require high sampling devices, application of neural network includes large training efforts and tedious testing procedures. The fault location algorithms for multi-terminal parallel transmission lines are proposed in [28], [29]. However, the efficacy of the aforementioned algorithms may not be ascertained in case of double/triple phase to ground faults. Consequently, synchronized voltage and current measurement based faulty segment categorization and fault distance approximation techniques are presented in [30], [31].

This paper proposed a novel faulty section identification and fault location method based on synchronized measurements from three ends of TTL. It works in the absence

This work is supported by Fulbright-Nehru Academic and Professional Excellence Fellowship having an Award No. 2351/F-NAPE/2018.

Vishal Kumar Gaur and Bhavesh R. Bhalja are with Department of Electrical Engineering, Indian Institute of Technology Roorkee, India (e-mail: vishalgaur_mait@yahoo.co.in, bhaveshbhalja@gmail.com)

Mladen Kezunovic is with Department of Electrical & Computer Engineering, Texas A&M University, USA. (e-mail: kezunov@ece.tamu.edu)

of synchronized measurement by calculating the value of synchronization operators to form a common reference among the three ends. The main benefit of the presented technique over several recently published techniques is that it has consistent accuracy throughout the line for all types of faults. It overcomes the issue of high sampling rate, data synchronization error, and miscalculations during complex fault impedance. Although the method is framed for homogeneous TTL, it can be applied to non-homogeneous TTL, two-terminal, and transposed as well as un-transposed lines. Test results obtained for the diverse scenarios reveal that the proposed technique is robust and accurate against wide variations in fault parameters, errors in line parameters, synchronization errors, and presence of noise in the measured signals. The performance of the proposed technique is minimally affected by an initial guess. It maintains an almost equal convergence rate for all types of fault except a case of CT saturation during an internal fault for which the convergence of the iterative process may take a greater number of iterations. The next section describes the mathematical derivation of synchronization operators and indices. Then, the performance of the proposed algorithm is evaluated in Section III for different fault cases and wide variations in system parameters. Section IV discusses the comparative evaluation of the proposed algorithm with several existing techniques. Lastly, Section V concludes the paper.

II. Proposed Fault Location Method

The single-line diagram of TTL, as a part of an existing Indian 400 kV power transmission network of the western grid, is shown in Fig. 1. It is equipped with PMUs at S, T and R terminals. The line section between terminals S, R and T and the junction point (M) is named as SM, RM, and TM, respectively, having a length of L_S, L_R, and L_T, in that order. The system parameters are depicted in the Appendix section. The modeling of the said network has been carried out in PSCAD/EMTDC software package based on the actual system data gathered from the substations [32].

A. Derivation of indices

The proposed method is based on the derivation of three indices, namely D_S, D_T, and D_R, which corresponds to a hypothetical fault spot in the line section SM, TM, and RM, correspondingly. It is noteworthy that the derivation of indices utilizes only a positive sequence network. Therefore, it is obvious that each variable mentioned in derivation refers to its positive sequence value. The value of D_S can be calculated by assuming a hypothetical fault at point F in the section SM. Based on the concept of transfer matrix [33], the voltage and current at the junction point with reference to terminal R and T, respectively, are given by,

$$\begin{bmatrix} \vec{U}_M^R \\ \vec{I}_M^R \end{bmatrix} = \begin{bmatrix} A_{RM} & B_{RM} \\ C_{RM} & D_{RM} \end{bmatrix} \begin{bmatrix} \vec{U}_R \\ \vec{I}_R \end{bmatrix} \text{ and } \begin{bmatrix} \vec{U}_M^T \\ \vec{I}_M^T \end{bmatrix} = \begin{bmatrix} A_{TM} & B_{TM} \\ C_{TM} & D_{TM} \end{bmatrix} \begin{bmatrix} \vec{U}_T \\ \vec{I}_T \end{bmatrix} \quad (1)$$

where,

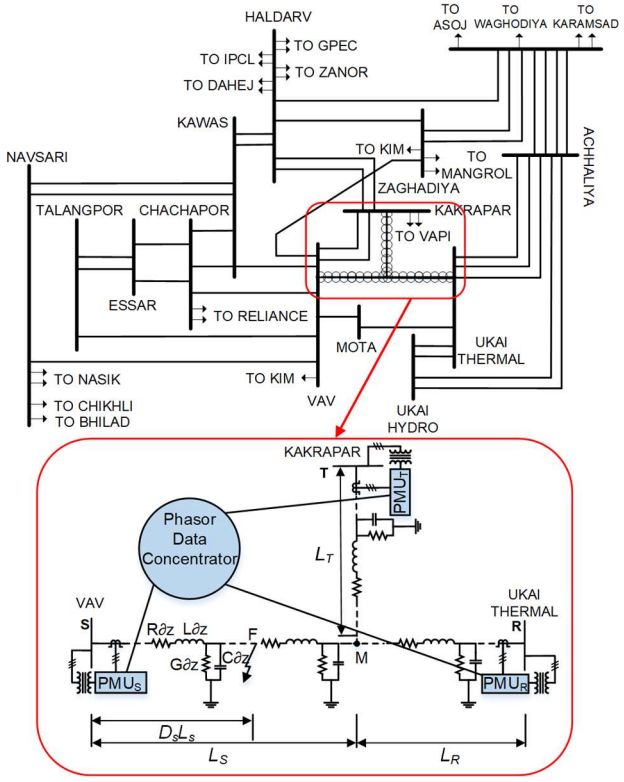

Fig. 1. One-line diagram of an existing Indian 400 kV system with TTL

$$\begin{bmatrix} A_{RM} & B_{RM} \\ C_{RM} & D_{RM} \end{bmatrix} = \begin{bmatrix} \left(e^{-\gamma_{RM}L_R} + e^{\gamma_{RM}L_R}\right)/2 & Z_{C,RM}\left(e^{-\gamma_{RM}L_R} - e^{\gamma_{RM}L_R}\right)/2 \\ \left(e^{-\gamma_{RM}L_R} - e^{\gamma_{RM}L_R}\right)/2Z_{C,RM} & \left(e^{-\gamma_{RM}L_R} + e^{\gamma_{RM}L_R}\right)/2 \end{bmatrix}$$

$$\begin{bmatrix} A_{TM} & B_{TM} \\ C_{TM} & D_{TM} \end{bmatrix} = \begin{bmatrix} \left(e^{-\gamma_{TM}L_T} + e^{\gamma_{TM}L_T}\right)/2 & Z_{C,TM}\left(e^{-\gamma_{TM}L_T} - e^{\gamma_{TM}L_T}\right)/2 \\ \left(e^{-\gamma_{TM}L_T} - e^{\gamma_{TM}L_T}\right)/2Z_{C,TM} & \left(e^{-\gamma_{TM}L_T} + e^{\gamma_{TM}L_T}\right)/2 \end{bmatrix}$$

Here, $\vec{U}_R$ & $\vec{U}_T$ and $\vec{I}_R$ & $\vec{I}_T$ are the voltage and current at terminal R and T, respectively. $\vec{U}_M^R$ & $\vec{U}_M^T$ are the voltage at the junction point M calculated using ABCD parameters of the line section RM and TM, respectively. Similarly, $\vec{I}_M^R$ & $\vec{I}_M^T$ are the currents transferred to the junction point M from terminal R and terminal T, respectively, which is calculated using ABCD parameters of the line section RM and TM, correspondingly.Further, $\gamma_{SM/RM/TM} = \sqrt{y_{SM/RM/TM} \times z_{SM/RM/TM}}$ and $Z_{C,SM/RM/TM} = \sqrt{z_{SM/RM/TM}/y_{SM/RM/TM}}$ are the propagation constant and the characteristic impedance of the line section SM, RM and TM, respectively. $z_{SM/TM/RM}$ and $y_{SM/TM/RM}$ are the per-unit series impedance and shunt admittance of the line section SM, TM, and RM, respectively.

Subsequently, current phasors $\vec{I}_M^R$ and $\vec{I}_M^T$ are given by (2) and (3), respectively.

$$\vec{I}_M^R = e^{-\gamma_{RM}L_R}\left(\frac{\vec{U}_R + Z_{C,RM}\vec{I}_R}{2Z_{C,RM}}\right) - e^{\gamma_{RM}L_R}\left(\frac{\vec{U}_R - Z_{C,RM}\vec{I}_R}{2Z_{C,RM}}\right) \quad (2)$$

$$\vec{I}_M^T = e^{-\gamma_{TM}L_T}\left(\frac{\vec{U}_T + Z_{C,TM}\vec{I}_T}{2Z_{C,TM}}\right) - e^{\gamma_{TM}L_T}\left(\frac{\vec{U}_T - Z_{C,TM}\vec{I}_T}{2Z_{C,TM}}\right) \quad (3)$$

It is noteworthy to mention that the calculated value of voltage at the junction point from terminal R ($\vec{U}_M^R$) and terminal T ($\vec{U}_M^T$) would be the same for a hypothetical fault in the line section SM which is expressed as,

$$\left.\begin{aligned}\vec{U}_M^R &= e^{-\gamma_{RM}L_R}\left(\frac{\vec{U}_R + Z_{C,RM}\vec{I}_R}{2}\right) + e^{\gamma_{RM}L_R}\left(\frac{\vec{U}_R - Z_{C,RM}\vec{I}_R}{2}\right)\\ \vec{U}_M^T &= e^{-\gamma_{TM}L_T}\left(\frac{\vec{U}_T + Z_{C,TM}\vec{I}_T}{2}\right) + e^{\gamma_{TM}L_T}\left(\frac{\vec{U}_T - Z_{C,TM}\vec{I}_T}{2}\right)\end{aligned}\right\} \quad (4)$$

Now, the fault point voltage with reference to terminal *S* ($\vec{U}_F^S$) and *M* ($\vec{U}_F^M$) are given by (5) and (6), respectively.

$$\vec{U}_F^S = e^{-\gamma_{SM}D_SL_S}\left(\frac{\vec{U}_S + Z_{C,SM}\vec{I}_S}{2}\right) + e^{\gamma_{SM}D_SL_S}\left(\frac{\vec{U}_S - Z_{C,SM}\vec{I}_S}{2}\right) \quad (5)$$

$$\vec{U}_F^M = e^{-\gamma_{SM}(1-D_S)L_S}\left(\frac{\vec{U}_M^R + Z_{C,SM}\vec{I}_M^{R,T}}{2}\right) + e^{\gamma_{SM}(1-D_S)L_S}\left(\frac{\vec{U}_M^R - Z_{C,SM}\vec{I}_M^{R,T}}{2}\right) \quad (6)$$

Where, $\vec{I}_M^{R,T}$ $(= \vec{I}_M^R + \vec{I}_M^T)$ is the estimated current at *M* flowing towards terminal *S* with reference to terminals *R* and *T*. D_S is the fault index of hypothetical fault spot with reference to terminal *S* in terms of per unit distance. In this regard, based on (5) and (6), a new non-linear equation is given by,

$$f(D_S) = \vec{U}_F^S - \vec{U}_F^M \quad (7)$$

The solution of equation (7) in terms of unknown D_S can be obtained using the iterative Newton method that starts with an initial guess of the root, *i.e.,* $D_S = D_S^i\big|_{i=1}$ for equation (7). Then, the next improved root (D_S^{i+1}) would be estimated as per (8) [34]. Here, *i* is the iteration count.

$$D_S^{i+1} = D_S^i - \frac{f(D_S^i)}{f'(D_S^i)} \quad (8)$$

where, $f'(D_S^i) = \frac{1}{2}\gamma_{SM}L_S[\vec{U}_S G - HZ_{C,SM}\vec{I}_S - \vec{U}_M^R J - KZ_{C,SM}\vec{I}_M^{R,T}]$,

$G = (e^{\gamma_{SM}D_S^iL_S} - e^{-\gamma_{SM}D_S^iL_S})$, $H = (e^{\gamma_{SM}D_S^iL_S} + e^{-\gamma_{SM}D_S^iL_S})$

$J = (e^{-\gamma_{SM}(1-D_S^i)L_S} - e^{\gamma_{SM}(1-D_S^i)L_S})$

and $K = (e^{\gamma_{SM}(1-D_S^i)L_S} + e^{-\gamma_{SM}(1-D_S^i)L_S})$

Once the difference between successive roots is smaller than the predefined tolerance limit (ε) or the maximum iteration count number, the iterative process stops. It is described in the literature that the computed phasor has maximum error immediately after the inception of fault due to several factors [35]. However, the presence of higher number of pre-fault samples (limited number of post-fault samples) in the data window also triggers such discrepancy in the computed phasor. The error will be reduced when sufficient number of post-fault samples are available. The above problem is more pronounced in case of occurrence of an internal fault on the line with CT saturation condition. In this case, the convergence of iterative process may take a greater number of iterations. In order to tackle this issue, the proposed algorithm stops the iterative process for the corresponding sampling instant once it reaches the maximum count. The obtained result of this instant will be discarded as it has not satisfied the tolerance limit. Afterward, the proposed algorithm tries to achieve a solution for the next sampling instant.

A similar process can be repeated for calculation of D_T and D_R. The relationship among these indices, used to identify the faulty line section and fault distance estimation, is shown in Table I. It is to be noted that length L_S, L_T and L_R will be considered as the reference length for calculation of D_S, D_T and D_R, respectively. In this regard, fault location in the line section SM, TM, and RM can be determined at a distance of D_SL_S, D_TL_T, and D_RL_R, respectively, away from terminal *S*, *T*, and *R*, in that order.

TABLE I
CRITERION FOR FAULTY SECTION IDENTIFICATION AND ESTIMATION OF FAULT LOCATION

Criterion	Faulty section	Fault location (km)
$0 < D_S < 1$, and D_T, $D_R > 1$	SM	$D_S L_S$
$0 < D_T < 1$, and D_S, $D_R > 1$	TM	$D_T L_T$
$0 < D_R < 1$, and D_S, $D_T > 1$	RM	$D_R L_R$
$D_S \approx D_T \approx D_R \approx 1$	Junction point M	$D_S L_S \approx D_T L_T \approx D_R L_R$

B. Derivation of the angle synchronization operator

Before proceeding with estimation of fault distance, it is necessary to establish a common time reference by measuring signals from all three terminals [36], [37]. If the time axis (local time reference) at terminals R and T lags (it can lead also) the reference time axis of terminal S by time $t_{\delta R}$ (or δ_R) and $t_{\delta T}$ (δ_T), respectively, then the pictorial representation of this situation is shown in Fig. 2. In this regard, the voltage and current at terminal S, R and T are given as per (9), (10) and (11), respectively.

$$\vec{U}_S = U_S\, e^{j\theta_{US}},\ \vec{I}_S = I_S\, e^{j\theta_{IS}} \quad (9)$$

Where, (U_S, θ_{US}) and (I_S, θ_{IS}) are the magnitude and phase angle of voltage and current measured at terminal S, respectively.

$$\left.\begin{aligned}\vec{U}_R^{unsyn} &= U_R\, e^{j(\theta_{UR}-\delta_R)} = \vec{U}_R^{Syn} e^{-j\delta_R}\\ \vec{I}_R^{unsyn} &= I_R\, e^{j(\theta_{IR}-\delta_R)} = \vec{I}_R^{Sync} e^{-j\delta_R}\end{aligned}\right\} \quad (10)$$

$$\left.\begin{aligned}\vec{U}_T^{unsyn} &= U_T\, e^{j(\theta_{UT}-\delta_T)} = \vec{U}_T^{Syn} e^{-j\delta_T}\\ \vec{I}_T^{unsyn} &= I_T\, e^{j(\theta_{IT}-\delta_T)} = \vec{I}_T^{Syn} e^{-j\delta_T}\end{aligned}\right\} \quad (11)$$

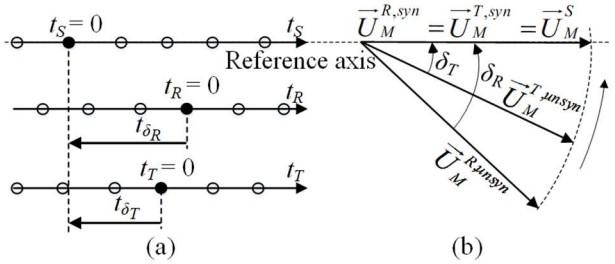

Fig. 2. (a) Local time axis at terminals S, T and R (b) phasor representation of tap-point voltage with synchronized and unsynchronized measurements

Where, ($\vec{U}_R^{unsyn}$, $\vec{I}_R^{unsyn}$) and ($\vec{U}_T^{unsyn}$, $\vec{I}_T^{unsyn}$) are the unsynchronized voltage and current measurements at terminal R and T, respectively. ($\vec{U}_R^{syn}$, $\vec{I}_R^{syn}$) and ($\vec{U}_T^{syn}$, $\vec{I}_T^{syn}$) are synchronized voltage and current at terminal R and T, respectively. (θ_{UR}, θ_{IR}) and (θ_{UT}, θ_{IT}) represent the phase angle of synchronized voltage and current at terminal R and T, respectively. Synchronization operators, δ_R and δ_T , are the phase angle lag of unsynchronized measurements corresponding to terminal R and T, respectively, with reference to terminal S.

These operators can be obtained by calculating junction point voltage $\vec{U}_M^S$, $\vec{U}_M^{R,unsyn}$ and $\vec{U}_M^{T,unsyn}$ with reference to terminal S, R and T, respectively, using (12), (13) and (14), correspondingly.

$$\vec{U}_M^S = \vec{U}_S A_{SM} - \vec{I}_S B_{SM} \tag{12}$$

where, $\vec{U}_M^S$ is the calculated value of junction-point voltage with respect to terminal S.

$$\begin{aligned}\vec{U}_M^{R,unsyn} &= \vec{U}_R^{unsyn} A_{RM} - \vec{I}_R^{unsyn} B_{RM} \\ &= (\vec{U}_R^{syn} A_{RM} - \vec{I}_R^{syn} B_{RM}) e^{-j\delta_R} = \vec{U}_M^{R,syn} e^{-j\delta_R}\end{aligned} \tag{13}$$

$$\text{Similarly,} \vec{U}_M^{T,unsyn} = \vec{U}_M^{T,syn} e^{-j\delta_T} \tag{14}$$

where, ($\vec{U}_M^{R,unsyn}$, $\vec{U}_M^{T,unsyn}$) and ($\vec{U}_M^{R,syn}$, $\vec{U}_M^{T,syn}$) are calculated values of junction -point voltage with reference to terminals R and T, respectively, by utilizing unsynchronized and synchronized measurements, in that order.

It is to be noticed from Fig. 2 (b) that $\vec{U}_M^S$, $\vec{U}_M^{T,syn}$ and $\vec{U}_M^{R,syn}$ would be equal during pre-fault conditions. Hence, the expression of δ_R and δ_T is derived from (12)-(14) and given by (15) and (16), respectively.

$$\delta_R = -\arg\left(\vec{U}_M^{R,unsyn} \Big/ \vec{U}_M^S\right) \tag{15}$$

$$\delta_T = -\arg\left(\vec{U}_M^{T,unsyn} \Big/ \vec{U}_M^S\right) \tag{16}$$

C. Proposed method

Utilizing 4 kHz sampling frequency with reference to 50 Hz fundamental frequency, phase voltage, and current samples are acquired at all terminals of TTL by instrument transformers. These samples are utilized by PMUs for phasor computation at all three terminals [38]. Then, the phasor values at each terminal are used for the calculation of positive sequence current and voltage phasors as per (17). The PMU, connected at each terminal of TTL, transfers the positive sequence voltage and current phasors to Phasor Data Concentrator (PDC) with a data reporting rate of 50 frames/s [39].

$$\left.\begin{aligned}\vec{I}_1 &= \frac{1}{3}(\vec{I}_A + a\vec{I}_B + a^2\vec{I}_C) \\ \vec{U}_1 &= \frac{1}{3}(\vec{U}_A + a\vec{U}_B + a^2\vec{U}_C)\end{aligned}\right\} \tag{17}$$

Where, subscript 1 indicates the positive-sequence component and $a = 1\angle 120°$. Further, subscript *A*, *B*, and *C* denotes phase quantities. The PDC located at the central monitoring station collects the synchrophasor data available from all the three terminals. Then, PDC decapsulates and synchronizes the data using calculated values of δ_R and δ_T. The synchronized data is utilized for calculation of D_S, D_T, and D_R. Finally, the tasks of faulty line-section identification and estimation of fault distance are carried out based on the criteria given in Table I.

III. Performance Evaluation

Though large numbers of simulation cases are generated with varying fault and system parameters, only few cases are described in this section. The percentage fault distance estimation error (also known as relative error based on the line length) has been calculated as per (18).

$$\text{Error (\%)} = \frac{|\text{estimated location-actual location}|}{\text{length between terminal S and R}} \times 100 \tag{18}$$

The IEEE C37.114™-2014 standard [6] has prescribed three methods for determining the fault location namely the absolute error, traditional relative error and relative error based on the line length. The relative error based on the line length has been used by the proposed method as this error is independent of the fault location.

A. Estimation of synchronization angles

The validity of equations (15)-(16) are evaluated by simulating different conditions of power flow during pre-fault condition. Based on the results obtained from the simulation as well as from analytical calculations (as per (15)-(16)), the values of δ_R and δ_T are given in Table II. It is inferred from Table II that the maximum error for estimation of both the synchronization angles remains below 0.2%.

B. Internal faults

Results of the proposed algorithm, in terms of three indices, during LG fault with R_F = 1 Ω at 10 km from terminal S and LLG fault with R_F = 100 Ω at 80 km from terminal R occurred at 0.6 s are depicted in Fig. 3 (a) and (b), respectively. As observed in Fig. 3 (a), the index D_S goes below unity whereas other two indices stay well above 1.0 indicating the faulty line-section SM as per the criteria given in Table I. The

TABLE II
ESTIMATION OF SYNCHRONIZATION ANGLE

Pre-fault condition	Synchronization angle (degree)					
Power transfer angle (degree)	δ_T (degree)			δ_R (degree)		
	Actual	Calculated	|Error| (%)	Actual	Calculated	|Error| (%)
θ_{US} = -10 θ_{UR} = -40 θ_{UT} = -15	-10	-9.99	0.08	+15	+14.99	0.07
	+15	+14.99	0.07	-10	-9.99	0.08
θ_{US} = -10 θ_{UR} = -25 θ_{UT} = -15	-15	-14.98	0.13	-10	-9.99	0.08
	+10	+9.99	0.09	-10	-9.99	0.08
θ_{US} = -40 θ_{UR} = -10 θ_{UT} = -25	+5	+4.99	0.16	-10	-9.99	0.08
	+20	+19.99	0.05	+5	+4.99	0.14
θ_{US} = -40 θ_{UR} = -10 θ_{UT} = -35	-12	-11.98	0.17	-8	-7.99	0.11
	+16	+15.99	0.06	-14	-13.98	0.14

estimated value of fault distance is 10.9 km ($D_S \times L_{SM}$ = 0.109×100) away from terminal S. Similarly, as witnessed from Fig. 3 (b), the value of indices D_S, D_T, and D_R are 1.199, 1.402 and 0.798, respectively. Hence, RM is identified as the faulty line section and the estimated value of fault distance is 79.8 km ($D_R \times L_{RM}$ = 0.798×100) away from the terminal R.

Further, the result in case of a LLL fault at the junction point is depicted in Fig. 4. It is to be observed from Fig. 4 that all the three indices attain almost unity values. Hence, the fault location is determined at the junction-point as per the criteria described in Table I. Subsequently, the variation in all three indices for varying fault locations in all the three-line sections

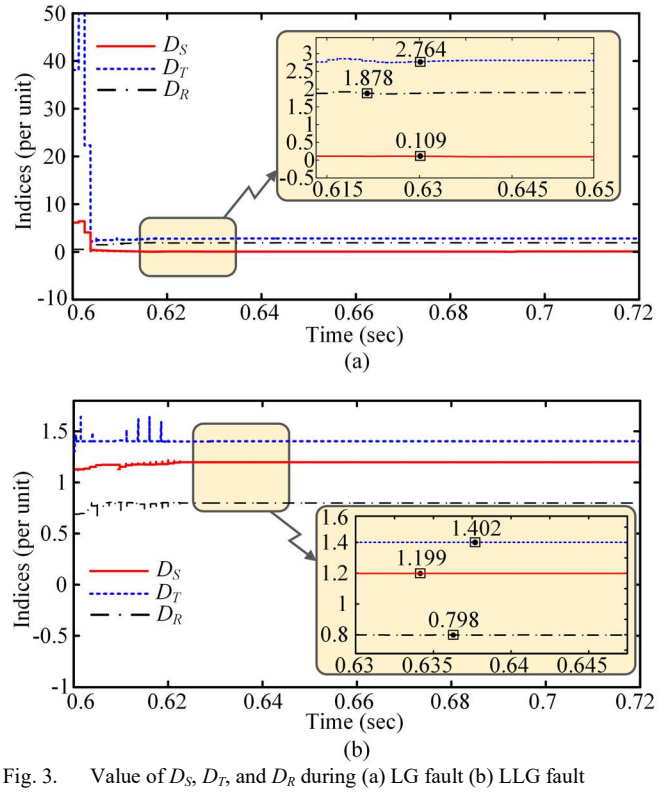

Fig. 3. Value of D_S, D_T, and D_R during (a) LG fault (b) LLG fault

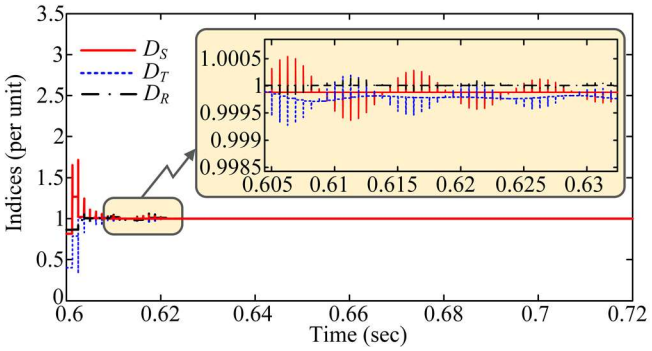

Fig. 4. Value of D_S, D_T, and D_R during a LLL fault at the tap-point

particularly near the junction point are depicted in Fig. 5. It is observed from Fig. 5 that the values of all indices approach unity as the fault location moves towards the junction-point. As observed from the zoomed portion of Fig. 5, the difference in indices at the junction point is of the order of 0.0008 per unit. The value of all indices can be round off up to 4th digit after the decimal with a tolerance value of ε = ±0.0002. It creates a zone around the junction-point for which every fault will be located at the junction point. This zone is marked and shown in Fig. 5 which is not more than 20.5 meters. Hence, the percentage fault location error of the proposed method due to this zone is of the order of 0.01%, which is very small.

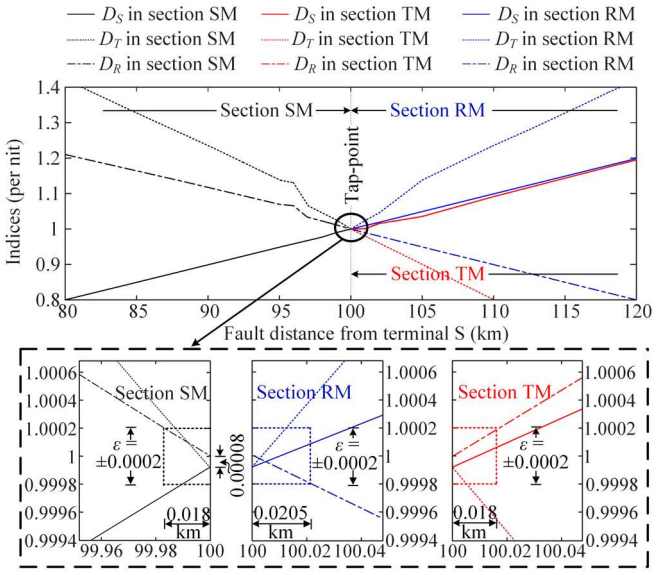

Fig. 5 Variation of indices near the junction point with varying fault location

C. *Influence of varying fault location and fault type*

Fig. 6 (a) and Fig. 6 (b) show the performance of the proposed method during ground faults (LG, LLG, LLLG with R_F = 200 Ω) and phase faults (LL and LLL) occurred at 0.6 s in line section SM with varying fault location. It is evident from both the figures that the maximum error for ground faults and phase faults is of the order of 0.1056% and 0.095%, respectively. Hence, it is concluded that the method delivers adequate results irrespective of fault type and varying fault locations.

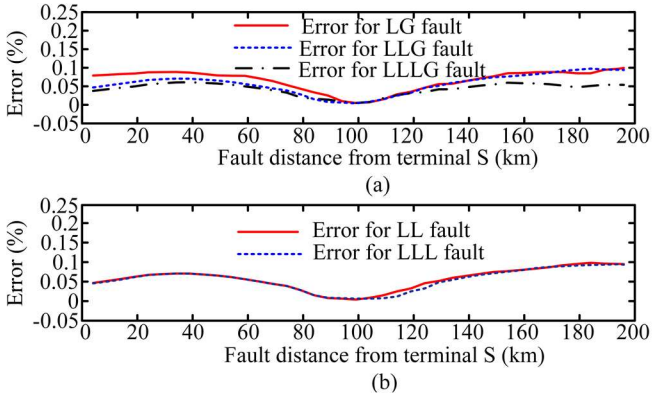

Fig. 6. Error during (a) ground faults and (b) phase faults

D. Impact of varying fault resistance and fault inception angle

Fault resistance may have a noticeable impact on the accuracy of fault location method. In order to investigate the effectiveness of the proposed method, various LG and LLG faults in the line section SM with variable R_F from 0.1 Ω to 150 Ω have been simulated at 0.6 s. Results in terms of fault distance estimation error are tabulated in Table III. It is observed from Table III that the maximum error is 0.11% for R_F =150 Ω. These results confirm the effectiveness of the proposed technique for high as well as low value of R_F. Similarly, the impact of varying fault inception angle (FIA) on the performance of the proposed method in terms of fault distance estimation error for various types of faults in the line section RM is summarized in Table IV. It is observed from Table IV that the fault location error stays below 0.25% irrespective of the value of FIA, which endorses the efficacy of the proposed technique.

TABLE III
FAULT DISTANCE ESTIMATION ERROR DURING VARYING FAULT RESISTANCE

R_F (Ω)	Fault distance (km) from terminal S	Fault distance estimation error (%)	
		LG	LLG
0.1	1	0.089	0.062
	90	0.066	0.058
5	1	0.087	0.065
	90	0.068	0.059
50	1	0.094	0.059
	90	0.089	0.07
150	1	0.110	0.078
	90	0.083	0.063

E. Impact of un-transposed TTL

In this case, modeling of three-line sections SM, RM, and TM has been changed from transposed line to un-transposed line. The performance of the proposed method in terms of maximum fault distance estimation error during ground faults (LG, LLG with R_F = 50 Ω and LLLG with R_F = 10 Ω) and phase faults (LL and LLL), simulated at 0.6 s, are depicted in Fig. 7. As observed in Fig. 7, the proposed approach yields consistent performance for un-transposed TTL as the maximum fault distance estimation error remains below 0.2% for all types of fault.

TABLE IV
FAULT DISTANCE ESTIMATION ERROR DURING VARYING FAULT INCEPTION ANGLE

FIA (degree)	Fault distance (km) from terminal R	Fault distance estimation error (%)			
		LG	LLG	LL	LLLG
0	15	0.095	0.083	0.091	0.089
	95	0.042	0.048	0.049	0.051
40	15	0.113	0.094	0.093	0.097
	95	0.074	0.065	0.078	0.071
80	15	0.225	0.148	0.126	0.094
	95	0.091	0.082	0.085	0.083
120	15	0.101	0.097	0.094	0.092
	95	0.076	0.072	0.077	0.074
160	15	0.099	0.093	0.131	0.112
	95	0.058	0.052	0.061	0.053

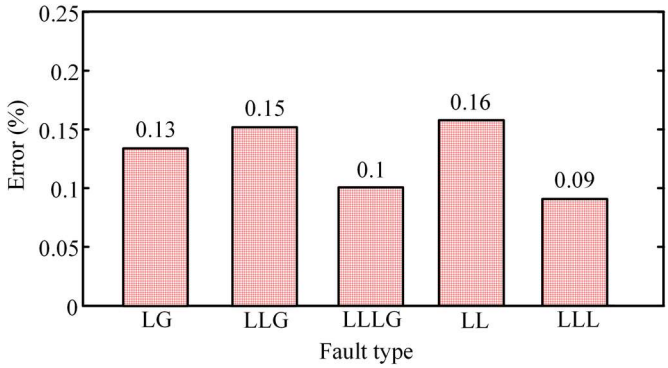

Fig. 7. Impact of un-transposed TTL on percentage error

F. Effect of synchronization error

Synchronization error corresponds to angle mismatch in data of one terminal with respect to data of other terminals. As per the IEEE C37.118.1-2011 standard, the time mismatch ($t_{SynchError}$) is determined by the need to match the requirement for a maximum of 1% of Total Vector Error (TVE) that corresponds to ±31 μs or 0.57 degree [39]. For different ground and phase faults occurring at 0.6 s in the line section SM, phase angle error of 0.57 degree is introduced in the data measured at T and R terminals. The maximum fault distance

TABLE V
FAULT DISTANCE ESTIMATION ERROR CONSIDERING SYNCHRONIZATION ERROR

Fault type	**Maximum fault location error (%)**			
	Proposed method	[24]	[28]	[29]
Ground faults (LG/LLG/LLLG)	0.77	0.94	1.93	2.11
Phase faults (LL/LLL)	0.81	1.02	2.17	2.32

estimation error given by the proposed scheme along with other schemes [24], [28] and [29] are depicted in Table V. The results indicate that the accuracy of the proposed method is comparatively better than the accuracy given by other methods.

G. *Effect of noise in the measurements*

The measurement data in the actual field are distorted due to transducers and environmental noise. In order to replicate the actual field data, a white Gaussian noise having different values of signal-to-noise ratio (SNR): 20, 30 and 40 dB is incorporated in the measured data. Various fault cases have been studied for different fault locations. Fig. 8 shows the maximum percentage error among all the simulated LLL faults at 0.6 s. It is to be noted from Fig. 8 that though the maximum percentage error increases, its value remains less than 5% even with worst-case i.e., SNR = 20 dB.

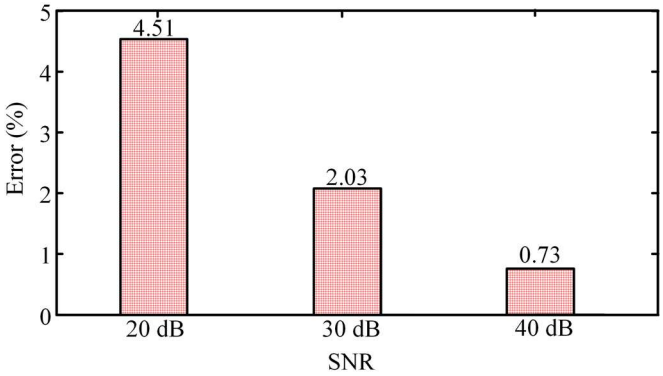

Fig. 8. Response of the proposed scheme considering noise in measurements

H. *Influence of errors in line parameters*

The impact of errors in line parameters on the accuracy of the proposed method are investigated by introducing 1%, 5%, and 10% errors. The results in terms of maximum fault distance estimation error along with other existing methods [10], [24], [28], and [29] during various ground and phase faults are reported in Table VI. It is observed from Table VI that unlike other methods, the maximum fault distance estimation error given by the proposed method remains less than 5% even with 10% errors in line parameters.

TABLE VI
PERFORMANCE EVALUATION OF THE PROPOSED METHOD IN CASE OF ERRORS IN LINE PARAMETERS

Errors in Line parameters (%)	**Maximum fault distance estimation error (%)**				
	Proposed method	[10]	[24]	[28]	[29]
1	0.14	1.55	0.23	0.45	0.33
5	2.39	4.17	3.31	3.43	4.76
10	4.78	8.43	5.87	6.99	7.12

I. *Impact of the initial guess on convergence and accuracy of the proposed algorithm*

Though Newton's method has the property of fast convergence, its accuracy depends on the initial guess and tolerance limit. In order to decide the initial guess, a comprehensive study has been performed by varying initial guess (0.1 to 1 in steps of 0.1) and fault location (0 to 1 per unit in steps of 0.1). The variation in fault distance estimation error against different values of initial guess and fault location during a LG fault in the line section SM is depicted in Fig. 9. Results shown in Fig. 9 depict that the accuracy of the proposed method is affected marginally as the error remains less than 0.5 % irrespective of initial guess. As a higher value of initial guess results in higher error, the initial guess of 0.1 per unit is selected for all the cases. At the same time, it is observed that with any value of initial guess between 0.1 and 1, the proposed technique entails only 3 iterations for converging the algorithm with a tolerance limit of 10^{-3}. It is worthwhile to note that change in tolerance limit to any value between 10^{-4} and 10^{-7} does not significantly reduce fault distance estimation error. Further, in case of tolerance limit < 10^{-7}, the convergence time or the number of iterations rises from 3 to more than 10. At the same time, for tolerance limit > 10^{-3}, the accuracy of the method decreases significantly.

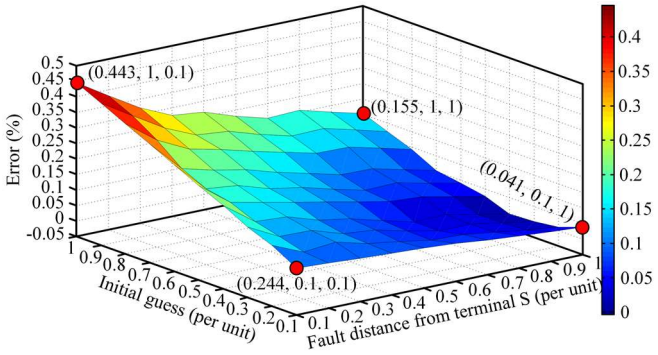

Fig. 9. Response of the proposed scheme for varying initial guess and fault location

J. *Impact of change in source impedance*

Owing to different reasons or due to outage of nearby transmission lines, the source impedance value may vary. In order to check efficacy of the proposed algorithm, equivalent source impedance behind all the three terminals (S, T and R) has been changed from 4 times to one-half times with reference to their original values (as given in Appendix). Results given by the proposed technique along with other techniques in terms of fault distance estimation error for a LLG fault at 0.6 s at a distance of 0.5 km from terminal S are shown in Table VII. It can be inferred from Table VII that the error given by the proposed technique is lower than 0.4% compared to higher value of error given by several existing techniques.

TABLE VII
COMPARISON OF THE PROPOSED METHOD WITH OTHER METHODS DURING CHANGE IN SOURCE IMPEDANCE

Change in source impedance with respect to original value at terminal			Fault distance estimation error (%)				
S	T	R	Proposed method	[10]	[24]	[28]	[29]
4 times	½ times	½ times	0.35	4.56	1.02	3.17	2.58
4 times	2 times	½ times	0.38	3.97	0.94	3.21	2.23
½ times	4 times	2 times	0.39	4.62	1.07	3.14	2.29
½ times	2 times	4 times	0.36	4.44	1.12	3.18	2.27

K. Impact of CT saturation

In numerical/digital relays, CT saturation leads to an error in phasor estimation especially for conventional methods. This leads to inaccurate estimation of fault location.

As the proposed scheme has used Modified Discrete Fourier Transform (MDFT) algorithm for phasor estimation of current signals [38], it estimates the phasors with smooth transient response, minimal overshoot and fast settling time (even considering the effect of noise present in the signal). However, it is also true that none of the phasor estimation algorithm can neutralize the effect of CT saturation completely. At the same time, the probability of CT saturation is more prominent in case of heavy short circuit (LL and LLL fault), which includes a significant decaying DC component. The effect of CT saturation can be reduced to a great extent if due care is taken while designing and choosing an accuracy class of CT cores. As 85–90% faults on overhead transmission lines are single line to ground (LG), a saturation of CT for such type of fault can be neglected due to minimum level of short circuit current compared to the level of fault current during heavy short circuit faults (LL and LLL). Subsequently, protection engineers are more concerned about saturation of CT particularly during external faults [40].

The performance of the proposed algorithm has been evaluated by simulating an internal three-phase fault at 0.6 s in the line section SM (5 km from terminal-S). The CT secondary burden has been increased to simulate the effect of saturation of the CT core. Fig. 10 (a) and (b) shows the corresponding three-phase current waveforms and indices, respectively. The line section SM is chosen as a faulty section, and D_S shows the per-unit fault distance with respect to

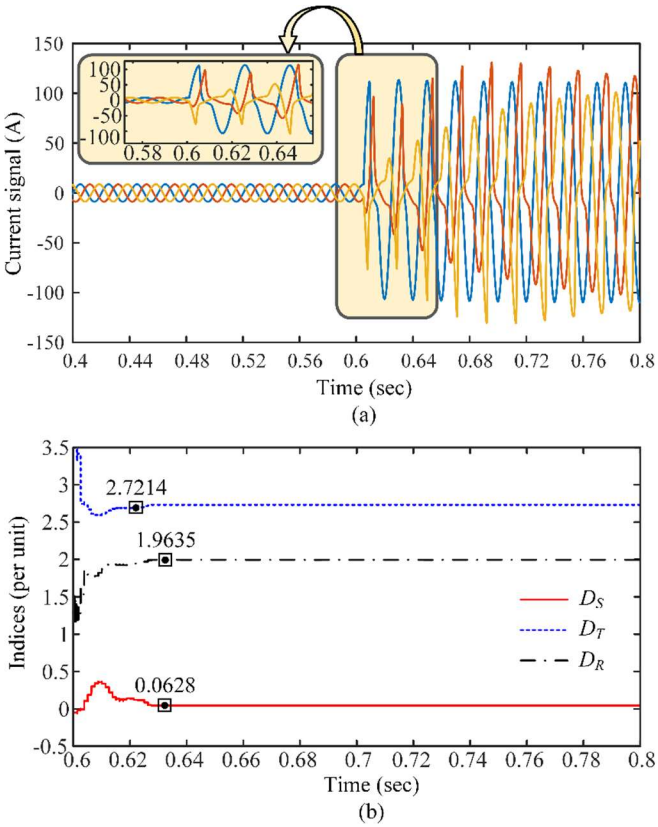

Fig 10. Performance of the proposed scheme with CT saturation (a) CT secondary current signal at terminal S (b) calculated value of Indices

terminal S which is 0.0628 per unit or 6.28 km (0.0628×100) with a percentage error of 0.14. Furthermore, the results during faults in three different line sections at various locations with CT saturation are summarized in Table VIII. It is to be noted from Table VIII that the proposed algorithm estimates the location of fault accurately and the maximum error is of the order of 0.684 in case of a LLL fault at 5% from terminal T. The aforementioned results indicate that the proposed scheme provides acceptable fault distance estimation accuracy even with considerable CT saturation.

L. Non-homogeneous (mixed) transmission lines

In certain cases, the system may consist of non-homogeneous AC transmission lines which are composed of different line parameter sections, such as underground cables in conjunction with overhead lines [29]. The proposed algorithm can be extended for non-homogeneous TTL with minor modifications. Fig. 11 shows a single line diagram of a

TABLE VIII
PERFORMANCE OF THE PROPOSED ALGORITHM FOR CLOSE-IN FAULTS WITH CT SATURATION

Fault type	Fault location error (%)								
	Fault from terminal S in line section SM at distance of			Fault from terminal T in line section TM at distance of			Fault from terminal R in line section RM at distance of		
	5%	7%	10%	5%	7%	10%	5%	7%	10%
LLL	0.64	0.612	0.579	0.684	0.622	0.549	0.621	0.614	0.581
LL	0.609	0.593	0.571	0.648	0.614	0.562	0.609	0.603	0.575
LLLG	0.64	0.612	0.575	0.682	0.593	0.544	0.617	0.608	0.577
LLG	0.611	0.593	0.572	0.661	0.585	0.537	0.594	0.597	0.564
LG	0.634	0.61	0.568	0.636	0.583	0.534	0.611	0.595	0.569

non-homogeneous TTL. In Fig. 11, line section SM consists of two sub-sections i.e. one overhead line (SJ) and the other is underground cable (JM). Similarly, the other two line-sections (RM and TM) are also divided into two sub-sections.

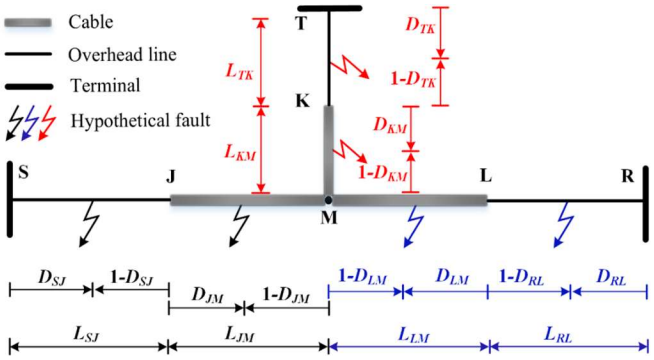

Fig. 11 Single line diagram of the non-homogeneous TTL

In order to calculate the fault location, indices corresponding to each sub-section are derived in a similar way as calculated in Section II A for homogeneous TTL. Hence, the total six indices i.e. D_{SJ}, D_{JM}, D_{RL}, D_{LM}, D_{TK}, and D_{KM}, are determined. The criterion for identification of faulty line section and fault distance calculation is depicted in Table IX. According to the criteria given in Table IX, the results of the proposed algorithm for faults in non-homogeneous TTL are shown in Table X. It is observed from Table X that the proposed algorithm is able to estimate the location of fault on non-homogeneous TTL accurately as the error remains less than 0.5%.

M. Impact of communication errors

The communication error occurs due to latency and data packet loss [41], [42].

(1) Latency: It occurs due to (i) variation in processing window with reference to data reporting rate, bandwidth/baud rate and the class of PMU, and (ii) transportation of data. The transportation latency depends on the physical length of the communication link and the medium of communication. It can be ignored as its value is of the order of micro-seconds [42]. Conversely, the latency due to variation in processing window includes time taken by a packet (all bits of a message) from analog input time instant to the instant at which digital output is available from PMU. For the proposed algorithm with a dedicated communication link for TTL, as shown in Fig. 1, positive sequence voltage and current (two signals) need to be transferred by each PMU. As each signal consists of 1 start bit, 1 stop bit, 8 data bits, and no parity bit, the total 20 bits (10 bits/signal) are required to be transferred corresponding to each message (or sampling instant). For a data reporting rate of 50 frames/s (or packets/s) with a sampling frequency of 4 kHz, the total number of messages per frame is 80. Considering conventional channel bandwidth of 64 kbps, the time required to transfer a message is around 1.25 ms (80/64000). Hence, the total time required or latency per frame to reach a destination (PDC) would be around 100 ms (80 messages per frame × 1.25 ms per message). Though the latency experienced by PMUs located at different terminals may not be the same, the PDC can easily align the data received from PMUs as long as it is time-stamped using GPS clock. In case of unavailability of GPS, each PMU transfers the data to the PDC with a local time-stamp. Hence, the data with a local time-stamp received at PDC need to be

TABLE IX
CRITERION FOR FAULTY SECTION IDENTIFICATION AND ESTIMATION OF FAULT LOCATION

Criterion	Faulty section		Fault location (km)
	Line section	Sub line section	
$0 < D_{SJ} < 1$, $D_{JM} < 0$ $(D_{TK}, D_{KM}, D_{RL}, D_{LM}) > 1$	SM	SJ	$D_{SJ}L_{SJ}$
$0 < D_{JM} < 1$ $(D_{SJ}, D_{TK}, D_{KM}, D_{RL}, D_{LM}) > 1$		JM	$L_{SJ} + D_{JM}L_{JM}$
$0 < D_{TK} < 1$, $D_{KM} < 0$ $(D_{SJ}, D_{JM}, D_{RL}, D_{LM}) > 1$	TM	TK	$D_{TK}L_{TK}$
$0 < D_{KM} < 1$ $(D_{TK}, D_{SJ}, D_{JM}, D_{RL}, D_{LM}) > 1$		KM	$L_{TK} + D_{KM}L_{KM}$
$0 < D_{RL} < 1$, $D_{LM} < 0$ $(D_{SJ}, D_{JM}, D_{TK}, D_{KM}) > 1$	RM	RL	$D_{RL}L_{RL}$
$0 < D_{LM} < 1$ $(D_{RL}, D_{SJ}, D_{JM}, D_{TK}, D_{KM}) > 1$		LM	$L_{RL}+D_{LM}L_{LM}$
$D_{JM} \approx D_{KM} \approx D_{LM} \approx 1$	Fault is at the junction-point		

TABLE X
RESPONSE OF THE PROPOSED METHOD FOR THREE-TERMINAL NON-HOMOGENEOUS TRANSMISSION LINES

Fault condition			Results		
Fault parameters	Faulty section	Fault distance	Value of indices (p.u.)	Faulty section identified	Fault distance error (%)
LLL fault at 0.605 s	TK	5 km from terminal T	D_{SJ} = 2.89, D_{JM} = 1.866 D_{TK} = 0.202, D_{KM} = -0.721 D_{RL} = 2.877, D_{LM} = 1.881	TK	0.025
LG fault with R_F = 50 Ω at 0.605 s	KM	15 km from point K	D_{SJ} = 2.246, D_{JM} = 1.323 D_{TK} = 1.567, D_{KM} = 0.6112 D_{RL} = 2.245, D_{LM} = 1.324	KM	0.14
LLG fault at 0.605 s	RL	25 km from terminal R	D_{SJ} = 3.533, D_{JM} = 2.527 D_{TK} = 4.92, D_{KM} = 4.111 D_{RL} = 0.5089, D_{LM} = -0.513	RL	0.2225
LG fault with R_F = 50 Ω at 0.605 s	LM	40 km from point L	D_{SJ} = 2.289, D_{JM} = 1.23 D_{TK} = 2.48, D_{KM} = 1.44 D_{RL} = 1.825, D_{LM} = 0.8062	LM	0.155

synchronized with reference to the local time corresponding to a terminal. This can be achieved by deriving synchronization angles to form a common time reference as discussed in Section II B. Once the synchronization angle is calculated, the data received from different terminals can be time-aligned as in case of synchronized measurements. Hence, the accuracy of the proposed algorithm is minimally affected due to latency effect. However, lateness (due to latency) in receiving data from other remote terminals would delay the process of execution of the relay algorithm.

(2) Data packet loss: Data packet loss is defined as the event when PMU data stream does not reach its desired destination. Though data packet loss depends on multiple factors, majorly two reasons can be attributed [41],[42]. The first reason is network congestion which results in less queuing time for the subsequent packets. The second reason is due to transmission error (bit error). These data packet losses may adversely affect some of the real-time applications in which PMU data are used. However, this paper has not considered the impact of congestion/data packet loss.

N. Computation time

The proposed algorithm utilizes a sampling frequency of 4 kHz (80 samples/cycle). In this regard, the computation time available between two consecutive samples or data windows is 0.25 ms (250 μs). The total computation time of an algorithm or data structure operation depends on the total number of arithmetic operations involved in the algorithm, hardware, and software [43]. In the proposed algorithm, the non-linear equations are solved using iterative methods to obtain the value of indices. The total number of operations to calculate the three indices using the proposed algorithm would be around 6697 [44]. It is to be noted that the number of primitive operations can be further reduced by utilizing optimized coding of algorithm in high-level language. For TMS320XXX signal processor (TI family, 40 MHz to 1200 MHz clock, 32-bit, floating-point), the execution of the proposed algorithm with 6697 arithmetic operations would take around 167 μs (using the minimum clock frequency of 40 MHz). Hence, the execution time of the proposed algorithm is lower than the time between two consecutive samples (250 μs). Further, with the faster signal processor of the same family (available at present up to 1200 MHz), the execution time of the algorithm may reduce to 5.56 μs [45], [46].

IV. Comparative Evaluation

Comparative evaluation of the proposed method with other existing methods on several aspects are depicted in Table XI. The proposed technique offers the following advantages when compared to other methods:

- For a LG fault at 50 km from terminal S (at 0.6 s) with $Z_F = 1 + j10$ Ω, the proposed method provides better accuracy (as the error is only 0.09%).
- In case of close-in LG faults (at 0.6 s) at 0.1, 0.5 and 2 km from terminal S, the maximum fault location error given by the proposed method is very small (0.12%) .
- The proposed scheme can accurately estimate fault location with an error of 0.02% during a high resistance LG fault with $R_F = 100$ Ω at 0.6 s near or at the junction point.
- Its performance is minimally affected due to noise in the measurement signals as it yields the lowest error (4.51%).
- It is suitable for all types of faults, reduced influence of synchronization errors and line parameter variations, and applicability for both transposed as well as un-transposed lines.
- It provides better accuracy (fault location error stays below 5%) even when considering high value of errors (10%) in line parameters.

V. Conclusion

A novel faulty section identification and fault distance

TABLE XI
COMPARATIVE EVALUATION OF THE PROPOSED METHOD WITH OTHER METHODS

Criterion			Proposed Method	[10]	[23]	[24]	[28]	[29]
Fault distance estimation error (%)	Complex fault impedance (Z_F =1 + j10)		0.09	1.32	12.75	0.13	14.2	0.94
	Close-in LG fault	0.1 km from terminal S	0.12	3.49	0.44	2.47	2.89	2.63
		0.5 km from terminal S	0.11	2.73	0.31	2.01	2.23	2.43
		2 km from terminal S	0.04	1.89	0.26	1.86	1.42	1.77
	High resistance fault at junction-point		0.02	1.95	0.09	0.17	0.27	0.06
	Effect of noise (SNR=20 dB)		4.51	8.77	6.83	6.49	8.16	8.43
Applicability for all types of fault (Yes: Applicable and No: Not Applicable) & Requirement of fault type identification (Yes: Required and No: Not required)			Yes & No	No & No	Yes & Yes	Yes & No	Yes & No	Yes & No
Maximum fault location error (%) considering 10% errors in line parameters			4.78	8.43	7.19	5.87	6.99	7.12
Modeling of line			Distributed parameters	Lumped parameters	Distributed parameters	Distributed parameters	Lumped parameters	Distributed parameters

estimation technique for TTL is presented in this paper. Considering distributed parameters and utilizing synchronized measurements from all three terminals of the line, three indices have been derived for segment identification and estimation of fault location. The proposed scheme measures fault location accurately (as maximum error stays below 4.8%) even in case of presence of noise in measurements, errors in line parameters and synchronization, and wide variation in fault and source parameters. It also maintains almost consistent convergence rate for all types of fault except under CT saturation during an internal fault when the convergence requires more iterations. Subsequently, it provides better accuracy in locating faults when compared to other existing methods in case of complex fault impedance, close-in symmetrical fault and high resistance fault at the junction point. The suggested scheme is also applicable to three-terminal transposed/untransposed as well as non-homogeneous transmission lines. Unlike several existing techniques, it applies to all types of fault and does not require fault type identification. However, impact of data packet loss needs to be considered as a future research work.

APPENDIX

TABLE A.1
SYSTEM PARAMETERS

Source parameters	
$Z_{1\,(S/T/R)} = Z_{2\,(S/T/R)} = (0.55+j7.98)\ \Omega$, $Z_{0\,(S/T/R)} = (1.5+j23.98)\ \Omega$	
Line parameters	
Positive/negative sequence impedance	(0.032+j0.3184) Ω/km
Zero sequence impedance	(0.256+j1.174) Ω/km
Positive sequence capacitance (C_1)	0.01163 μF/km
Zero sequence capacitance (C_0)	0.0076764 μF/km
Zero sequence mutual impedance (Z_{0M})	(0.249+j1.172) Ω/km
Length of L_{SM}, L_{TM} and L_{RM} line section	100, 50 and 100, respectively, in (km)

REFERENCES

[1] *IEEE Guide for Protective Relay Applications to Transmission Line,* IEEE Std. C37.113-2015, 2016.

[2] A. A. Girgis, D. G. Hart and W. L. Peterson, "A new fault location technique for two- and three-terminal lines," *IEEE Trans. on Power Del.*, vol. 7, no. 1, pp. 98-107, January 1992.

[3] M. Abe, N. Otsuzuki, T. Emura and M. Takeuchi, "Development of a new fault location system for multi-terminal single transmission lines," *IEEE Trans. on Power Del*, vol. 10, no. 1, pp. 159-168, January 1995.

[4] S. Sarangi and A. K. Pradhan, "Adaptive direct under-reaching transfer trip protection scheme for the three-terminal line," *IEEE Trans. on Power Del.*, vol. 30, no. 6, pp. 2383-2391, Dec. 2015.

[5] IEEE Power System Relaying Committee, "Protection aspects of multi-terminal lines," *IEEE Publ. no. 79*, TH0056-2-PWR, 1979.

[6] *IEEE Guide for Determining Fault Location on AC Transmission and Distribution Lines*, IEEE Std. C37.114™-2014, 2014.

[7] I. Niazy and J. Sadeh, "A new single ended fault location algorithm for combined transmission line considering fault clearing transients without using line parameters," *Int. J. Elect. Power Energy syst*., vol. 44, no. 1, pp. 816-823, 2013.

[8] A. Esmaeilian and M. Kezunovic, "An impedance based fault location algorithm for tapped lines using local measurements," 2013 North American Power Symposium (NAPS), Manhattan, KS, 2013, pp. 1-6.

[9] M. Farshad and J. Sadeh, "Accurate single-phase fault-location method for transmission lines based on k-nearest neighbor algorithm using one end voltage," *IEEE Trans. On Power Del.*, vol. 27, no. 4, pp. 2360-2367, Oct. 2012.

[10] B. Mahamedi, M. Sanaye-Pasand, S. Azizi and J. G. Zhu, "Unsynchronized fault location technique for three-terminal lines", *IET Gen., Trans., Distrib.*, vol. 9, no. 15, pp. 2099-2107, June 2015.

[11] Mahmoud A. Elsadd, Almoataz Y. Abdelaziz, "Unsynchronized fault-location technique for two- and three-terminal transmission lines," *Elect. Power Syst. Res.*, vol. 158, pp. 228-239, May 2018.

[12] B. K. Chaitanya and A. Yadav, "Decision tree aided travelling wave based fault section identification and location scheme for multi-terminal transmission lines," *Measurement*, vol. 135, pp. 312-322, March 2019.

[13] J. Ding, X. Wang, Y. Zheng and L. Li, "Distributed traveling-wave-based fault-location algorithm embedded in multi-terminal transmission lines," *IEEE Trans. on Power Del*, vol. 33, no. 6, pp. 3045-3054, Dec. 2018.

[14] O. D. Naidu and A. K. Pradhan, "A traveling wave based fault location method using unsynchronized current measurements," *IEEE Trans. on Power Del.,* vol. 34, no. 2, pp. 505-513, April 2019.

[15] M. Davoudi, J. Sadeh and E. Kamyab, "Transient-based fault location on three-terminal and tapped transmission lines not requiring line parameters," *IEEE Trans. on Power Del.*, vol. 33, no. 1, pp. 179-188, February 2018.

[16] C. Y. Evrenosoglu and A. Abur, "Travelling wave based fault location for teed circuits," *IEEE Trans. on Power Del*, vol. 20, no. 2, pp. 1115-1121, April 2005.

[17] Z. Yongli and F. Xinqiao, "Fault location scheme for a multi-terminal transmission line based on current traveling waves," *Electr. Power & Energy Sys*; vol. 53, pp. 367-374, 2013.

[18] M. D. Silva, D. V. Coury, M. Oleskovicz and E. C. Segatto, "Combined solution for fault location in three-terminal lines based on wavelet transforms," *IET Gen. Trans. & Distrib*, vol. 4, no. 1, pp. 94-103, January 2010.

[19] V. R. K. Bhupatiraju and R. R. V. Pulipaka, "A wavelet based protection scheme for EHV asymmetrical teed circuits," *Proc. IPEC*, Singapore, 2010, pp. 384-389.

[20] A. Ahmadimanesh and S. M. Shahrtash, "Transient-based fault-location method for multiterminal lines employing S-Transform," *IEEE Trans. on Power Del.*, vol. 28, no. 3, pp. 1373–1380, July 2013.

[21] S. R. Samantaray, L. N. Tripathy and P. K. Dash, "Differential equation-based fault locator for unified power flow controller-based transmission line using synchronised phasor measurements," *IET Gen. Trans. & Distrib*, vol. 3, no. 1, pp. 86-98, January 2009.

[22] M. Mirzaei, B. Vahidi and S. H. Hosseinian, "Fault location on a series-compensated three-terminal transmission line using deep neural networks," *IET Sci. Meas. & Tech.*, vol. 12, no. 6, pp. 746-754, May 2018.

[23] Ying-Hong Lin, Chih-Wen Liu and Chi-Shan Yu, "A new fault locator for three-terminal transmission lines using two-terminal synchronized voltage and current phasors," *IEEE Trans. on Power Del*., vol. 17, no. 2, pp. 452-459, April 2002.

[24] C. W. Liu, K. P. Lien, C. S. Chen and J. A. Jiang, "A universal fault location technique for N-terminal (N ≥ 3) transmission lines," *IEEE Trans. on Power Del.*, vol. 23, no. 3, pp. 1366-1373, July 2008.

[25] J. Izykowski, E. Rosolowski, M. M. Saha, M. Fulczyk and P. Balcerek, "A fault-location method for application with current differential relays of three-terminal lines," *IEEE Trans. on Power Del.*, vol. 22, no. 4, pp. 2099-2107, October 2007.

[26] N. A. Al-Emadi, A. Ghorbani and H. Mehrjerdi, "Synchrophasor-based backup distance protection of multi-terminal transmission lines," *IET Gen. Trans. & Distrib.,* vol. 10, no. 13, pp. 3304-3313, April 2016.

[27] A. Esmaeilian and M. Kezunovic, "Fault location using sparse synchrophasor measurement of electromechanical wave oscillations," *IEEE Trans. Power Del.*, vol. 31, no. 4, pp. 1787–1796, August 2016.

[28] T. Funabashi, H. Otoguro, Y. Mizuma, L. Dube, A. Ametani, "Digital fault location for parallel double-circuit multi-terminal transmission lines," *IEEE Trans. on Power Delivery*, vol. 15, no.2, pp. 531-537, April 2000.

[29] A. Saber, A. Emam and H. Elghazaly, "A backup protection technique for three-terminal multisection compound transmission lines," *IEEE Trans. on Smart Grid*, vol. 9, no. 6, pp. 5653-5663, November 2018.

[30] S. M. Brahma, "New fault-location method for a single multi terminal transmission line using synchronized phasor measurements," *IEEE Trans. Power Del.,* vol. 21, no. 3, pp. 1148–1153, July 2006.

[31] V. K. Gaur and B. Bhalja, "New fault detection and localisation technique for double-circuit three-terminal transmission line," *IET Gen. Trans. & Distrib.*, vol. 12, no. 8, pp. 1687-1696, April 2018.
[32] User's Guide v4.6 of PSCAD/EMTDC, Manitoba HVDC Research Center, 2016.
[33] G. Manassero, E. C. Senger, R. M. Nakagomi, E. L. Pellini and E. C. N. Rodrigues, "Fault-location system for multiterminal transmission lines," *IEEE Trans. on Power Del.*, vol. 25, no. 3, pp. 1418-1426, July 2010.
[34] J. Izykowski, R. Molag, E. Rosolowski and M. M. Saha, "Accurate location of faults on power transmission lines with use of two-end unsynchronized measurements," *IEEE Trans. on Power Del.*, vol. 21, no. 2, pp. 627-633, April 2006
[35] S. N. Ananthan, A. F. Bastos, S. Santoso, A. Del Rosso, "An automated technique for extracting phasors from protective relay's event reports," *Inventions,* vol. 3, no. 4, 2018, pp. 1-18.
[36] J. Izykowski, E. Rosolowski, P. Balcerek, M. Fulczyk and M. M. Saha, "Fault Location on Double-Circuit Series-Compensated Lines Using Two-End Unsynchronized Measurements," *IEEE Trans. on Power Del.*, vol. 26, no. 4, pp. 2072-2080, October 2011.
[37] M. M. Saha, J. J. Izykowski, and E. Rosolowski, *Fault Location on Power Networks* (Power Systems Series). London, U.K.: Springer-Verlag, 2010.
[38] K. M. Silva and F. A. O. Nascimento, "Modified DFT-based phasor estimation algorithms for numerical relaying applications," *IEEE Trans. on Power Del.*, vol. 33, no. 3, pp. 1165-1173, June 2018.
[39] *IEEE Standard for Synchrophasor Data Transfer for Power Systems*, IEEE Std. C37.118.2™-2011, 2011.
[40] Z. Xu, M. Proctor, I. Voloh and M. Lara, "CT saturation tolerance for 87L applications," *68th Annual Conference for Protective Relay Engineers*, Texas A&M, 2015, pp. 646-671.
[41] P. NASPI, "PMU Data Quality: A framework for the attributes of pmu data quality and quality impacts to synchrophasor applications," 2017.
[42] R. Khan, K. McLaughlin, D. Laverty, and S. Sezer, "IEEE C37.118- 2 synchrophasor communication framework - overview, cyber vulnerabilities analysis and performance evaluation," *2nd International Conference on Information Systems Security and Privacy*, 2016.
[43] A. G. Phadke, and J. S. Thorp, "Communication needs for wide area measurement applications," *5th IEEE International Conference on Critical Infrastructure*, Sep 20-22, 2010, pp. 1-7.
[44] R. N. Jat, D. S. Ruhela, "Comparative study of complexity of algorithms for ordinary differential equations," *Journal of International Academy of Physical Sciences*, vol. 15, no. 4, pp. 455-466, 2011.
[45] M. Kezunovic, I. Rikalo, and D. J. Sobajic, "Neural network applications to real-time and off-line fault analysis," *Intl. Conf. on Intelligent System Applications to Power Systems*, France, Sept. 1994.
[46] W. Rebizant, J. Szafran, A. Wiszniewski. *Digital Signal Processing in Power System Protection and Control*. Springer, New York, 2008.

VI. BIBLIOGRAPHIES

Vishal Kumar Gaur (S'17) received B.Tech. from MAIT, Delhi, India, and M.Tech. from SVNIT, Surat, India in 2011 and 2014, respectively. He is currently working toward the Ph.D. degree with the Department of Electrical Engineering, Indian Institute of Technology Roorkee, Roorkee, India. His research interests include digital protection of power system.

Bhavesh Bhalja (M'07–SM'10) received the B.E. in electrical engineering and the M.E. in power system engineering from B.V.M. Engineering College, Sardar Patel University, Anand, India, in 1999 and 2001, respectively, and the Ph. D. from the Indian Institute of Technology (IIT) Roorkee, Roorkee, India, in 2007. He is currently working as an Associate Professor with the Department of Electrical Engineering, IIT Roorkee. He has authored and coauthored more than 100 papers in referred international journals. His research interests include digital protection and automation, smart grid technologies and applications, distributed generation, micro-grid and power quality improvement. Dr. Bhalja was the recipient of Fulbright-Nehru Academic and Professional Excellence Fellowships, the Young Engineers Award, the Merit Award, and the Pandit Madan Mohan Malviya Award by the Institution of Engineers, India.

Mladen Kezunovic (S'77–M'80–SM'85–F'99–LF'17) received the Dipl. Ing. from University of Sarajevo, Sarajevo, Bosnia, and M.Sc. and Ph.D. degrees in electrical engineering from University of Kansas, Lawrence, KS, in 1974, 1977, and 1980, respectively. He has been with Texas A&M University, College Station, TX, USA, for 33 years, where he is currently Regents Professor, Eugene E. Webb Professor, and the Site Director of "Power Engineering Research Center" consortium. He acted for over 25 years as the Principal Consultant of XpertPower Associates, a consulting firm specializing in power systems data analytics. His expertise is in protective relaying, automated power system disturbance analysis, computational intelligence, data analytics, and smart grids. He has authored over 600 papers, given over 120 seminars, invited lectures, and short courses, and consulted for over 50 companies worldwide. Dr. Kezunovic is a CIGRE Fellow, Honorary and Distinguished member. He is Registered Professional Engineer in Texas.